Nonlinear Influence of Background Rotation on Iceberg Melting

Agostino N. Meroni

December 17, 2017

1 Introduction

Iceberg dynamics and thermodynamics still include processes that are poorly understood. Indeed, there is lot of interest in comprehending the complex interactions between icebergs and their surrounding, both in terms of how the environment influences the iceberg and vice versa. In particular, the meltwater produced by icebergs themselves has been observed to modify the local ocean physical and chemical properties, affecting both the dynamical [17, 9] and the biogeochemical response [16, 4]. Moreover, icebergs are well known to pose a hazard for human activities such as oil platforms, submarine pipelines and, of course, navigation [3].

Recent numerical works have underlined the importance of correctly describing the iceberg size distribution in order to get the right climatology for sea-ice, ocean temperature and salinity [18, 14]. In particular around Antarctica, where large tabular icebergs with areas that can reach values up to $O(10^3 \text{ km}^2)$ exist, the incorrect size distribution representation, for example by neglecting these giant icebergs, can lead to a bias towards the South in the freshwater input [14].

For a comprehensive review of the mechanisms that control icebergs dynamics and melting, the reader is referred to [15, 1]. Contributions to the melting come both from surface processes and from subsurface ones, as depicted in figure 1. In particular, above the air-sea interface, solar radiation, forced convection due to the winds and sublimation take place, but they represent the least important mechanisms. At the interface, instead, the dominant mechanism, wave erosion, continuously acts and reduces the iceberg volume both by directly transferring heat from the seawater through the periodic wave motion and by inducing calving of the iceberg fraction above the sea level that is left because of the melting itself. Below the sea level then, buoyant and forced convection significantly contribute to the submarine melting by entraining relatively warmer oceanic water in the turbulent layer attached to the iceberg. The former is due to the vertical motion associated to the positively buoyant meltwater, while the latter is due to the relative motion of the water masses, as explained more in detail below [15].

Forced convection at the base of the iceberg is the mechanism studied in the present work. It refers to the transfer of heat between a fluid and a submerged body through the turbulent boundary layer that develops at the interface due to the relative fluid flow [5]. In the case of icebergs, the relative fluid motion is provided by the fact that their displacement is not always controlled by vertically uniform flow. Thus, for example, if there is a vertical shear in the current or if the wind drives the iceberg or if the iceberg

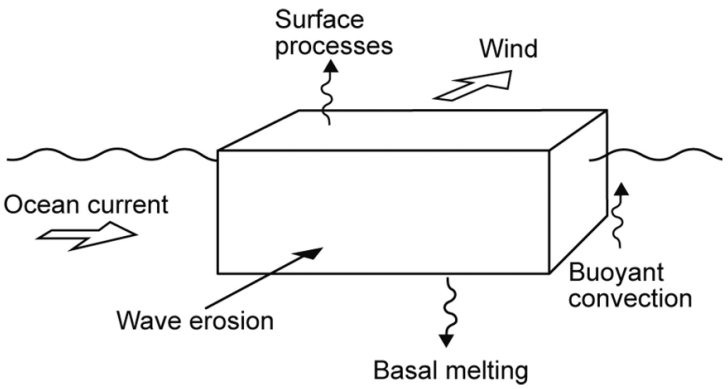

Figure 1: Schematic of the iceberg deterioration processes, adapted from [1].

gets stuck by some bathymetric feature, it is easy to imagine the presence of a relative flow with respect to the iceberg [1, 7].

Various efforts have been done to represent this kind of melting as a function of the fluid and ice properties (relative flow speed, fluid temperature and salinity, ice temperature), to better understand the relevant physical quantities involved in the process and, as an application, to capture this submarine melting in general circulation models (GCM). The two most widespread parameterizations are Weeks and Campbell (WC) [21] and the three equations [10], first developed for the basal ice shelf melting. Examples of the use of both schemes in GCM are [2] for the former and [20, 14] for the latter, among others. In general, though, there is evidence that the iceberg melting representation in GCMs is over-simplified and active research brings new insights in how such mechanisms work [6].

The goal of the present study is to quantify the effects of a background rotation on iceberg melting, if any. In section 2 some background information about the current iceberg melting parameterizations and the analytical solutions of the flow below a solid obstacle in a rotating frame of reference in simple configurations, leading to the so-called Taylor columns, is given. Section 3 is devoted to describing the experimental methods and setup to tackle the problem, the results of which are presented in section 4. Some remaining open issues and conclusions are given in section 5.

2 Background

2.1 Submarine melting parameterization

Following a similar experimental procedure to previous work [6], the focus is on the WC submarine melting parameterization [21] that describes the submarine melt rate per unit area SMR as a function of the relative flow speed U, the driving temperature $\Delta T = T_w - T_i > 0$ (with T_w denoting the water temperature and T_i denoting the ice temperature)

and the length scale of the iceberg in the direction of the flow ℓ as

$$\mathrm{SMR} = K\Delta T \frac{U^{0.8}}{\ell^{0.2}}, \tag{1}$$

where K is a constant of proportionality that contains various physical constants, as described in the following derivation [21].

The SMR is defined as the iceberg volume loss per unit area and per unit time. It can be written as

$$\mathrm{SMR} = \frac{\Delta V}{A\Delta t},$$

where ΔV is the volume loss, A is the area of the iceberg in contact with the fluid and Δt is the time interval considered. If the iceberg is already at its melting temperature and thus all the heat transferred from the fluid to the iceberg Q contributes to its melting, then with ρ_i denoting the ice density and L_i its latent heat of fusion, one can write

$$\mathrm{SMR} = \frac{Q}{L_i \rho_i A \Delta t}.$$

At this point, to generalize this relationship, one introduces the Nusselt number Nu that, over a length scale ℓ and for a fluid with thermal conductivity κ, is the nondimensional version of the heat per unit time, per unit area and per unit driving temperature transferred between the body and the fluid

$$q = \frac{Q}{A\Delta t \Delta T},$$

namely

$$\mathrm{Nu} = \frac{q\ell}{\kappa}. \tag{2}$$

This gives that the SMR scales with the Nusselt number as

$$\mathrm{SMR} = \frac{\Delta T \kappa}{L_i \rho_i \ell}\mathrm{Nu}. \tag{3}$$

But the scaling of the Nu with respect to the Reynolds number, $\mathrm{Re} = U\ell/\nu$, with ν being the fluid viscosity, and the Prandtl number, $\mathrm{Pr} = c_p \rho_w \nu/\kappa$, with c_p being the fluid specific heat and ρ_w its density, are known from past experimental works in the form

$$\mathrm{Nu} \simeq C\mathrm{Re}^m \mathrm{Pr}^n, \tag{4}$$

where the coefficients C, m, n depend on the geometry of the body and on the Re of the flow [5]. In this work, two geometrical configurations are considered: a flat plate, which has been used to derive the WC parameterization [21], and an infinite cylinder, for reasons that will be clarified in section 3. Table 1 contains the values of C, m, n for $\mathrm{Re} \sim 10^4$, which is consistent with the experimental setup described below. With the values for the flow past a flat plate, it is now clear that by using equation (4) in equation (3), the final form of the WC parameterization (1) is obtained.

As already mentioned, the WC parameterization has been applied both to numerical works [2] and experimental ones [6]. In particular, in the laboratory it has been possible

Geometry	C	m	n
Flat plate	0.037	0.8	0.33
Infinite cylinder	0.193	0.618	0.31

Table 1: Coefficients of the scaling of Nu as a function of Re and Pr as in equation (4) for Re$\sim 10^4$ and for two geometrical configurations [5].

to test its behavior for vanishing relative speed U, which is a limit where the free stream forced convection becomes a second order process and the melting is controlled by other mechanisms. For the lateral melting, it has been shown that the forced convection due to the buoyant plumes is the major process for low U [6]. This happens because the meltwater produced by the ice block itself, being buoyant due to its lower salinity content, moves upwards forming plumes along the sides of the block. Figure 2 shows that, for low relative velocity ($u < w_p$, where $w_p \simeq 2.5$ cm s $^{-1}$ is the characteristic vertical velocity of the plume), the melting is correctly parameterized using the buoyant plume temperature and velocity in the WC expression. While for higher velocity, $u > w_p$, the WC parameterization with the free stream quantities fits the data well. The schemes in the right panel of the same figure show the different behavior of the vertical plumes in the two regimes (A) and (C). In the former, the meltwater produced by the ice block at the ice-water interface forms buoyant plumes that remain attached to the ice block, which is thus unaware of the free stream flow. In the latter, instead, due to the higher free stream velocity, the plumes are swept away and the free stream velocity and temperature control the forced convection that melts the ice block. There is also an intermediate regime, marked with (B) in the left panel of the figure, that is intermediate between the two.

2.2 Taylor column dynamics

Since the goal of the work is to study the effects of background rotation on iceberg melting, the fluid dynamics in a rotating frame of reference past an obstacle is here revised in some simple configurations. In particular, it is well known that in a barotropic, inviscid, fast-rotating flow (in the sense of low Rossby number, as explained more in detail below), the velocity field is independent of the coordinate in the direction of the axis of rotation. In a system where the axis of rotation is vertical, this can be written as $\frac{\partial}{\partial z}\mathbf{u} = 0$

and implies that, if an obstacle is placed somewhere in the domain, the flow is forced to go around it not only at the depth where the obstacle is physically present, but also everywhere on top of (or below) it. It is as if the obstacle was virtually extended throughout the entire fluid column. The fluid that occupies this virtual volume remains stagnant and is a so-called Taylor column (TC) [19].

But this is the extreme case where the Coriolis time scale is much smaller than the advective one. In the range between the non-rotating case and this extreme one, the analytical solution for a cylindrical obstacle is now revised following [12, 13]. Consider a

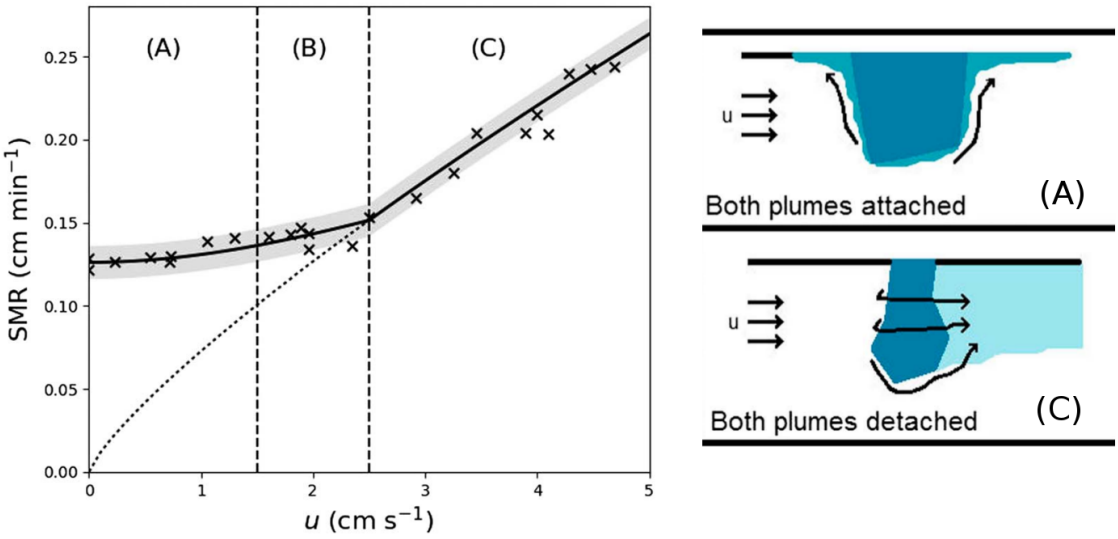

Figure 2: Left panel: lateral SMR as a function of the free stream velocity. The WC parameterization in regimes (A) and (B) is calculated with the plume temperature and velocity, while in regime (C) it uses the free stream ones. Right panel: schemes of the two regimes. (A) shows that for low relative speed the buoyant plumes shield the ice block from the fluid flow and the buoyant convection controls the lateral melting. (C) shows that for high relative speed the plumes are swept away and the forced convection controls the melting. Regime (B) is intermediate and the figure is adapted from [6].

homogeneous and constant fluid flow confined between two flat plates distant H from each other and rotating at a constant rate Ω, which sets a background constant absolute vorticity $f = 2\Omega$. Let U be the fluid velocity and choose a frame of reference with the x axis along the direction of the flow, with no loss of generality. If a flat-topped cylindrical obstacle of radius L and height $h \ll H$ is attached to one of the plates, defining the Rossby number as Ro$= U/fL$ and the nondimensional height of the obstacle as $h_0 = h/H$, the steady state flow dynamics at low Ro is determined only by the parameter

$$\alpha = \frac{\mathrm{Ro}}{h_0} = \frac{U}{fL}\frac{H}{h} \tag{5}$$

[12]. In particular, starting from a relatively large α, the presence of the obstacle affects the flow by bending the streamlines, following potential vorticity (PV) conservation. As an example, consider that the obstacle is attached to the upper plate. Then, by writing down the nondimensional linearized PV conservation equation as

$$\frac{D}{Dt}\left(\nabla^2\Psi + h_0\right) = 0, \tag{6}$$

where Ψ is the streamfunction, together with the far field conditions

$$u = -\partial\Psi/\partial y = \alpha \quad \text{and} \quad v = \partial\Psi/\partial x = 0 \quad \text{for} \quad x^2 + y^2 \to \infty, \tag{7}$$

it is easy to understand that if the background vorticity is positive ($f > 0$), the squeezing due to the obstacle ($h_0 > 0$) induces a negative (anticyclonic) component in the relative vorticity ($\nabla^2\Psi < 0$). As α increases, a stagnation point appears in the velocity field. It has been shown that the critical value for which this condition is reached depends on the geometry of the obstacle and on the stratification of the fluid [11]. For even lower values of α, then, a closed circular streamline below the obstacle appears. Its radius increases for decreasing α and it delimits a region of zero motion, the so-called Taylor column. The panels of the top row of figure 3 show these solutions for three different values of α.

Since, as clarified in the following, in the experimental setup there is a horizontal shear in the far field flow, the solution of the problem of the above is obtained in a very similar way for the case of horizontally sheared flow, by adding a second parameter, β, that controls the horizontal shear [13]. In particular, if the horizontal velocity changes by an amount ΔU over a cross-flow distance Δy, the new parameter is defined as

$$\beta = \frac{\Delta U/\Delta y}{f}\frac{H}{h} \tag{8}$$

and modifies the u velocity far field condition of equation (7) as

$$u = -\partial\Psi/\partial y = \alpha + \beta y. \tag{9}$$

For the rest, the problem is the same and it can be shown that the solutions differ whether the vorticity added by the horizontal shear has the same sign of the vorticity anomaly induced by the squeezing below the obstacle or the opposite. In the former case, the stagnation region is generated for values of α higher than the zero-shear critical one α_c, while in the latter, the Taylor column occurs for $\alpha < \alpha_c$.

Figure 3 shows the analytical steady solution of the TC problem outlined above, both for zero horizontal shear (top row) and for a positive one (bottom row). The parameters used to plot this figure are taken from the experimental setup as described in section 3. In the case of positive background rotation ($f > 0$), the direction of the flow along the streamlines (solid thin black) is from left to right, while for $f < 0$ it is from right to left. The top row is obtained for a uniform far field velocity $U = 4$ cm s^{-1}, while the bottom row for a positively sheared flow $U = U_0 + y\Delta U/\Delta y$, with $U_0 = 4$ cm s $^{-1}$ and $\Delta U/\Delta y = 0.1$ s^{-1}. The different columns correspond to different values of $\alpha = \mathrm{Ro}/h_0$ and for the geometry considered, the critical value at which the stagnation point in the zero-shear case appears is $\alpha_c = 0.5$ [11]. Panels (A), (D) have $\alpha = 1 > \alpha_c$ and do not have any TC, because the background rotation has a rather small effect on the flow and thus the difference between the velocity magnitude of the flow with respect to the far field (denoted with the color shading) is small. Panels (B), (E) have $\alpha = 0.5 = \alpha_c$ and in the zero-shear case, panel (B), the stagnation point at the lower end of the obstacle is visible in correspondence of the cusp in the appropriate streamline. Panel E shows that the presence of a positive shear makes it easier to have a region of no motion (delimited by the black dashed line), because the added background velocity due to the positive β is of the same sign of the vorticity anomaly induced by the squeezing of the fluid below the obstacle. Panels (C) and (F), then, have $\alpha = 0.25 < \alpha_c$ and they both show a region of zero motion, which has been shown to grow bigger for lower values of α [12]. It is interesting to notice that while on the lower side of the obstacle the region of zero motion appears, on the upper side there is a relative increase in velocity with respect to the far field profile.

To have a sense of the importance of such dynamics in the real oceans, the following typical values of the quantities defining α are considered. Take a relative speed of $U \sim 10$ cm s^{-1}, a Coriolis parameter of $f \sim 10^{-4}$ s^{-1}, a horizontal length scale of the iceberg of $L \sim 20$ km, a depth of the water of $H_w \sim 10^3$ m and a draft of the iceberg of $h_i \sim 500$ m. This leads to

$$\alpha = \frac{U}{fL}\frac{H_w}{h_i} \sim 10^{-1},$$

which is of the same order of magnitude of the critical value $\alpha_c = 0.5$ considered above, which motivates the current investigation because it shows that rotation can be important in the dynamics in the vicinity of an iceberg and, thus, can impact its melting.

3 Methods

The experiments were conducted in a rotating tank with a diameter of 210 cm and filled with seawater with salinity of roughly 33 g kg^{-1} kept at room temperature, $18 - 20$°C. At least 30 minutes before the beginning of each experiment, the rotating tank was turned on to set the fluid in solid body rotation with angular velocity Ω_0 and corresponding absolute vorticity $f_0 = 2\Omega_0$. The spin-up time that characterizes this transient fluid acceleration has been largely studied in the past [8] and is given by the expression

$$\tau_E = \frac{H}{(2\nu f_0)^{1/2}}, \tag{10}$$

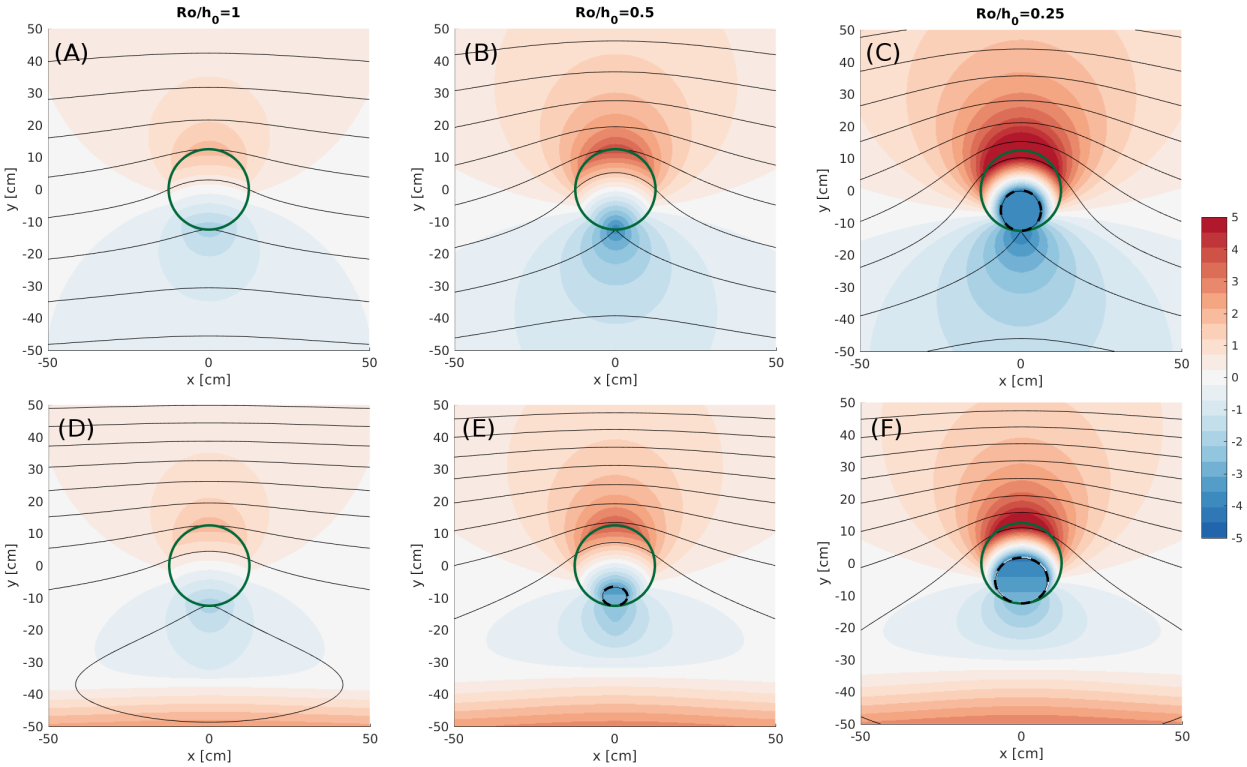

Figure 3: Top row, panels (A), (B), (C): analytical steady solution of the TC problem with zero horizontal shear for different values of $\alpha = \mathrm{Ro}/h_0$ [12]. Bottom row, panels (D), (E), (F): solution of the same problem and for the same values of α, but with positive horizontal shear with $\Delta U/\Delta y = 0.1$ s^{-1} [13]. The black solid thin lines are streamlines, while the color shading indicates the difference between the flow velocity magnitude and the far field velocity profile: constant and equal to 4 cm s^{-1} in the top row and increasing with y with $U(y = 0) = 4$ cm s^{-1} in the bottom row. The green solid line is the section of the cylindrical obstacle and the black dashed line in panels (C), (E) and (F) delimits the region of no motion predicted by the analytical solutions.

with H being the fluid column depth and ν its viscosity. The physics that controls this spin-up process involves the Ekman boundary layer at the bottom of the tank, which pushes the fluid far from the axis of rotation and, by mass conservation, brings fluid parcels with higher angular momentum, that accelerate the fluid throughout the tank, inwards.

Once the fluid was in solid body rotation, a cylindrical ice block of radius L was suspended in the water with a wooden support at a distance R from the axis of rotation and with a submerged part of height h (see figures 4 and 5). At this point, since the ice block was fixed in the frame of reference of the tank, two options were available to set a relative flow between the seawater and the ice block. The first consisted of increasing the rotation rate of the tank by a certain amount $\Delta\Omega$ at the beginning of the experiment, so that the relative flow speed at the center of the obstacle was initially $U_0 = R\Delta\Omega$. This resulted, according to the spin-up dynamics described before [8], in a relative flow decaying almost exponentially

$$U(t) \simeq U_0 \mathrm{e}^{-t/\tau_E} \tag{11}$$

in the frame of reference of the tank and the ice block. The second option, instead, consisted in increasing the rotation rate of the tank by a smaller amount $\delta\Omega < \Delta\Omega$ at regular intervals δt, calculated using the exponential decay above, so that the relative flow speed would be constant. In particular, using the equivalent of equation (11) for the angular velocity together with the expression of the spin-up time (10), the interval δt at which the tank acceleration is needed to balance the relative velocity, decay was found by inverting

$$\delta\Omega = \Delta\Omega \left(1 - \mathrm{e}^{-t/\tau_E}\right), \tag{12}$$

after choosing $\delta\Omega$ to be some fraction of $\Delta\Omega$. The choice for the experiments was $\delta\Omega = \Delta\Omega/10$, so that the values of δt were between 15 to 40 s, as a function of the initial background rotation, f_0. This procedure was tested for different values of f_0, R, $\Delta\Omega$ by measuring the fluid angular velocity with floating tracers and after a few trial and error tests, it was possible to keep the relative flow speed constant, with fluctuations of the order of 5% (not shown). Despite some experiments that were carried in the first configuration (constant f decaying U), all the data analyzed and shown in what follows come from the series of experiments with constant U and increasing f.

The ice blocks were made in stainless steel cylindrical molds with radius $L = 12.5$ cm and were roughly 5 cm tall, so that they could be half submerged during the experiments, resulting in values of $h \simeq 2$ or 3 cm. The water used to make the ice blocks was deaired and dyed with 2 ml blue food colorant in order to be able to distinguish the meltwater from the seawater of the tank. There are two reasons why the ice blocks were cylindrical. The former is because the focus of this work was on the basal iceberg melting rather than the lateral one. Thus, since the circle is the figure that maximizes the area for a given perimeter, the cylindrical shape has the highest basal-to-lateral area ratio for a given height. This means that it is the optimal choice to study the melting coming from the base and for the values of the experiments, $h \sim 2$ cm and $L = 12.5$ cm, the area of the base πL^2 is roughly three times larger than the area of the side $2\pi Lh$. The latter reason is because the analytical solutions for the TC problem, described in section 2.2, has been developed only for flat-topped cylindrical obstacles [12, 13].

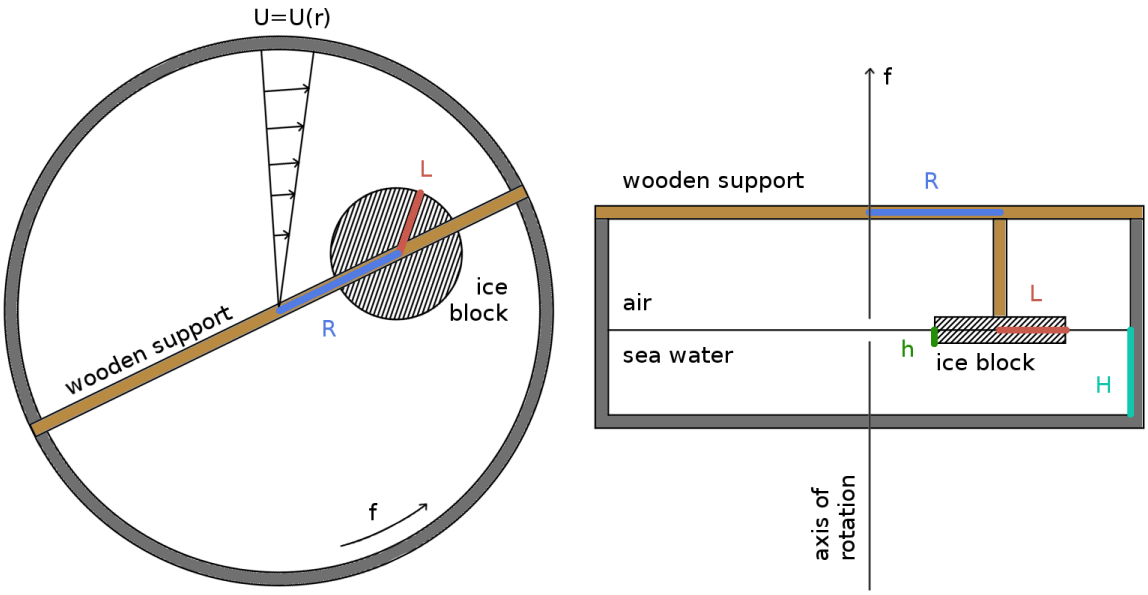

Figure 4: On the left, a top view schematic of the apparatus (not to scale), where the radially increasing relative velocity profile $U = U(r)$ in the frame of reference of the ice block is drawn. The distance of the center of the ice block (hatched) from the axis of rotation R, the radius of the ice block L and the direction of the rotation in the frame of reference of the laboratory f are marked, as well. On the right, a side view of the same apparatus is sketched with also the draft of the ice block h and the depth of the seawater H.

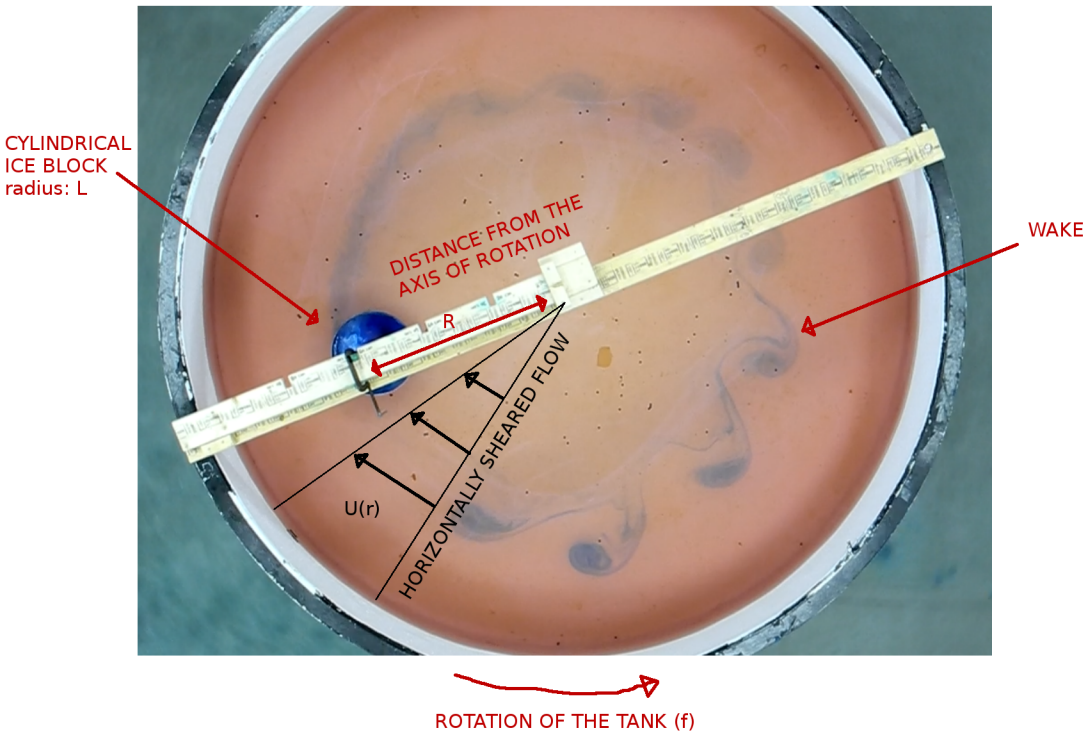

Figure 5: Top view picture of the apparatus during an experiment that shows how all the elements sketched in the previous schematic looked like in the laboratory.

Special attention was paid during the experiments with high background rotation rate because the water surface was free to adjust to the well known paraboloid shape reached at the balance between the centrifugal acceleration and the hydrostatic pressure gradient. Denoting with H_{eff} the effective height of the water as a function of the radial distance r from the axis of rotation and the rotation rate itself Ω, one can write

$$H_{eff}(r,\Omega) = H + \frac{\Omega^2}{4g}(2r^2 - D^2), \tag{13}$$

where g is the acceleration due to gravity, $D = 105$ cm is the radius of the rotating tank and H, the non-rotating value, was chosen to be equal to 12 cm. All the experiments, even those with the most tilted free surface, were conducted making sure that the upper side of the ice block was never submerged in order to avoid the introduction of an extra melting source.

For each experiment, two quantities were measured: the mass loss Δm and the initial submerged draft h_0. To understand how the SMR was obtained, let us consider a reasonable scenario in which the average radius of the cylindrical ice block $L = L(t)$ decreases linearly in time as

$$L(t) = L_0 - \dot{\delta}t \tag{14}$$

and the average submerged height as

$$h(t) = h_0 - \dot{\epsilon}t. \tag{15}$$

The lateral and basal ice block melt rates are thus

$$\frac{dL}{dt} = -\dot{\delta}, \quad \frac{dh}{dt} = -\dot{\epsilon}, \quad \text{with} \quad \dot{\delta}, \dot{\epsilon} > 0 \tag{16}$$

and supposing that they are constant one can write that over a time interval Δt the radius and the height decrease by an amount $\delta = \dot{\delta}\Delta t$ and $\epsilon = \dot{\epsilon}\Delta t$, respectively. Given the expressions (14) and (15), the submerged instantaneous area is

$$A(t) = \pi L(t)\left[L(t) + 2h(t)\right], \tag{17}$$

and the corresponding volume is

$$V(t) = \pi L^2(t)h(t), \tag{18}$$

which decreases in time with a rate

$$\frac{dV}{dt} = -\pi L(t)\left[L(t)\dot{\epsilon} + 2h(t)\dot{\delta}\right]. \tag{19}$$

This enables us to write the instantaneous SMR as

$$\mathrm{SMR}(t) = -\frac{1}{A(t)}\frac{dV}{dt} = \frac{L(t)\dot{\epsilon} + 2h(t)\dot{\delta}}{L(t) + 2h(t)} > 0. \tag{20}$$

It is now interesting to have a sense of how the side melt rate and the basal melt rate compare. To do so, the two different geometrical configurations (flat plate and infinite

cylinder) discussed in section 2.1 for the heat turbulent transfer are considered. If the side melt rate is taken to scale with the Re as if the flow was around an infinite cylinder and if the basal melt rate scales as if flow was past a flat plate, the ratio $\dot{\delta}/\dot{\epsilon}$ is

$$\frac{\dot{\delta}}{\dot{\epsilon}} \simeq 0.81, \tag{21}$$

using the coefficients of table 1, the typical velocity of the experiments $U = 4$ cm s^{-1} and the radius of the cylinder $L = 12.5$ cm as a length scale. This justifies the assumption

$$\dot{\delta} = \dot{\epsilon}, \tag{22}$$

which, if replaced in the expression (20), shows immediately that the SMR is constant and equal to

$$\mathrm{SMR} = \dot{\epsilon} = \dot{\delta}. \tag{23}$$

Over a time interval Δt, the ice block volume loss with the assumption $\delta = \epsilon$ is simply

$$|\Delta V| = \int_0^{\Delta t} \mathrm{d}t \left| \frac{dV}{dt} \right| = \pi \left[L_0^2 h_0 - (L_0 - \epsilon)^2 (h_0 - \epsilon) \right]. \tag{24}$$

Thus, the correct value of the area A^* to be used when calculating the SMR of the experiments in the form

$$\mathrm{SMR} = \frac{|\Delta V|}{A^* \Delta t} \tag{25}$$

can be inferred by inverting the above expression to get to the first order in ϵ

$$A^* = \pi \left[L_0 (L_0 + 2h_0) - \epsilon (2L_0 + h_0) \right]. \tag{26}$$

This, to same order in ϵ, can be shown with little algebra to be equal to the average area

$$A_{av} = \frac{1}{2} \left(A_{in} + A_f \right), \tag{27}$$

where

$$A_{in} = \pi L_0 (L_0 + 2h_0) \quad \text{and} \quad A_f = \pi (L_0 - \epsilon)[(L_0 - \epsilon) + 2(h_0 - \epsilon)]$$

are simply the initial and the final submerged ice block areas. Since from the measurements $\Delta V = \Delta m/\rho_i$, h_0 and L_0 are known, the two equivalent ways of obtaining the SMR from the experiments are to invert equation (24) to get ϵ and then find SMR as in equation (23) dividing ϵ by the duration of the experiment, or to calculate the average area of equation (27) imposing the same volume integral of equation (24) and then apply the definition (25) with $A^* = A_{av}$. Note that the duration of the experiments, $\Delta t = 3$ min, was chosen so that the final shape was still a quite regular cylinder and in the case of high background rotation rate, where the free surface was significantly tilted, the mean value of the submerged height of the cylinder was used to calculate the geometrical properties of the block. The time interval was short enough to linearize the evolution of the submerged area in time and, thus, to justify the truncation to the first order in ϵ of the expressions (26) and (27).

4 Results

In this section, the experimental data obtained from four series of experiments with different values of free stream velocity, $U \in \{0, 2, 4, 6\}$ cm s^{-1}, are described.

Figure 6 shows the SMR of all the experiments as a function of U. The data points are color-coded with the value of $\alpha = \mathrm{Ro}/h_0$ (except for $U = 0$ cm s^{-1}, where $\alpha = 0$ because Ro= 0), that controls the TC dynamics as described in section 2.2. The solid line shows the WC parameterization, as in equation (1), with $K = 0.052$, $\Delta T = 18°$C and $\ell = 2L = 25$ cm (note that here the diameter of the ice block is used). The value of K, as discussed in 2.1, contains several physical constants of the system and it is here chosen so that all the inputs of the parameterization are taken in S.I. units and the SMR is measured in cm min^{-1}. As for ΔT, it is taken as the difference between the seawater room temperature, 18°C, and the ice freezing temperature in freshwater, 0°C, because the temperature gradient between ice and seawater is much larger than their salinity gradient and thus, the ice is in a condition of pure melting with no dissolution. Physically, it means that a thin layer of freshwater insulates the ice block from the seawater, so that the salinity at the interface is zero and the freezing temperature is, accordingly, 0°C.

Back to figure 6, the experimental error is shaded along the parameterization to have an estimate of the uncertainty in the matching between the data and the parameterized line. The first evident feature is that for $U = 0$ cm s^{-1} and $U = 2$ cm s^{-1}, the SMR is much higher than the parameterized one, which is indicative of another process controlling the melting for low free stream velocity, as found in previous works [6]. The hypothesis is that at low U, the positively buoyant meltwater formed at the base of the ice block will flow as a gravity current faster than the free stream velocity. Unfortunately, due to the configuration of the experimental setup, it has not been possible to observe this processes at the base of the ice block accurately. Thus, further experiments with submerged cameras and/or in a non-rotating transparent tank are encouraged to better observe and understand what happens at the base of the block.

As a first simple attempt to include this basal meltwater pool process in the SMR dependence on the free stream velocity, a constant SMR below a certain threshold velocity U_{thr} was suggested. In particular, U_{thr} was calculated inverting the same WC parameterization as before,

$$\mathrm{SMR}_{U=0} = K\Delta T \frac{U_{thr}^{0.8}}{\ell^{0.2}} \tag{28}$$

assuming the SMR to be equal to the value obtained from the experiments at zero relative flow velocity, $\mathrm{SMR}_{U=0} = 0.09 \pm 0.01$ cm min^{-1}. The value obtained is $U_{thr} = 3.8 \pm 0.5$ cm s^{-1} and figure 7 shows the just mentioned constant SMR behavior below this threshold. Data points at high α (which means low rotation rate) of both the 4 cm s $^{-1}$ and 2 cm s^{-1} series agree quite well with this constant value.

Let us now focus on a single series of experiment with constant non-zero free stream velocity. A common feature that the three series with $U \in \{2, 4, 6\}$ cm s^{-1} share is that as α decreases, the SMR increases. The SMR as a function of α for $U = 4$ cm s $^{-1}$ is shown in figure 8. The data points, together with their uncertainty, are shown as green dots. The uncertainty on the SMR, $\sigma_{\mathrm{SMR}} = 0.01$ cm min^{-1}, is obtained from few repetitions of the same experiment and has then been extended to all the data points. While the uncertainty

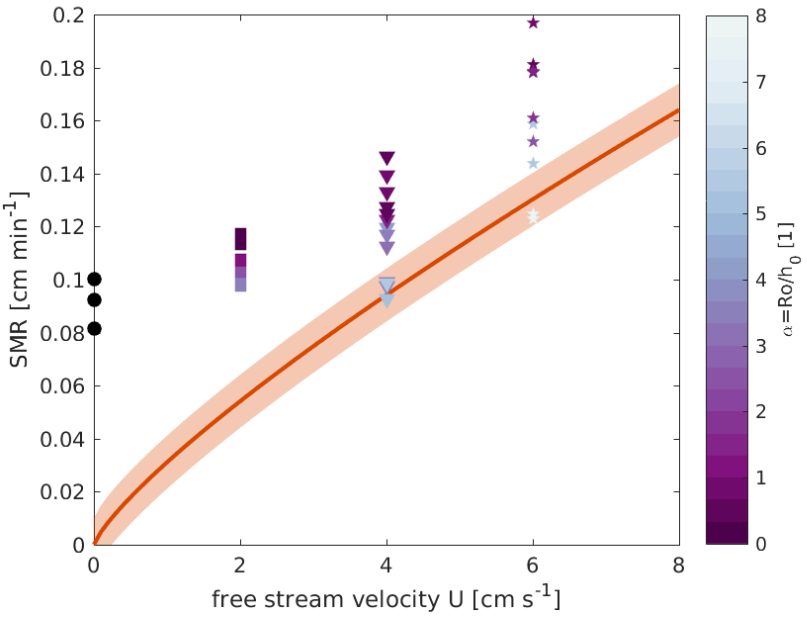

Figure 6: SMR as a function of the free stream velocity U for all the experiments considered. The WC parameterization of equation (1) is shown as a solid line with the experimental error shaded. The color of the data points is chosen according to the value of α of each experiment.

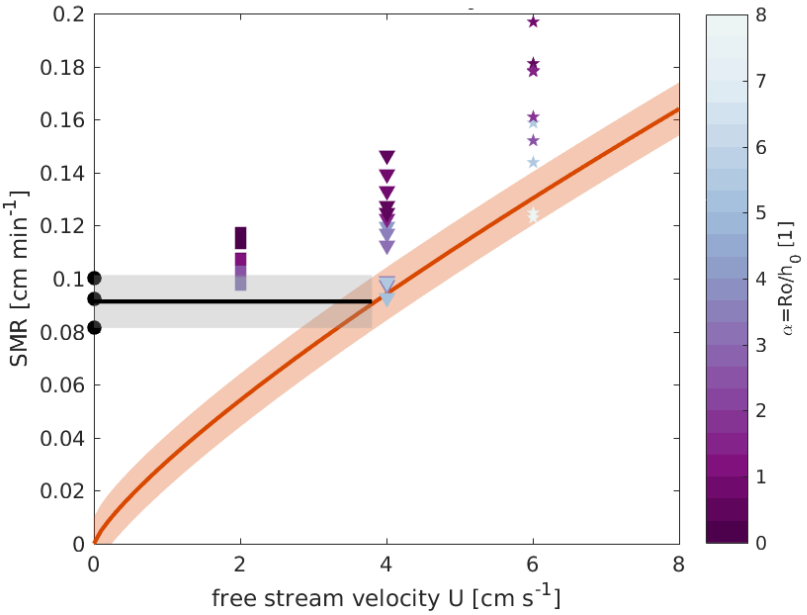

Figure 7: With respect to figure 6, a constant SMR line is added (black) in correspondence of the experimental value obtained with no relative flow, $\mathrm{SMR}_{U=0} = 0.09 \pm 0.01$ cm min^{-1}, for relative velocity below the threshold $U_{thr} = 3.8 \pm 0.5$ cm s^{-1}. See the text for further details.

on α comes both from the experimental uncertainty on h, the draft of the ice block, and from the fact that to maintain the relative velocity U constant, the rate of rotation had to increase throughout the experiment. In this figure, the significant increasing trend as α decreases, i.e. the background rotation increases, is visible. The black solid line denotes the value of the WC parameterization calculated as before, for $U = 4$ cm s^{-1}, which is constant because it does not depend anyhow on the background rotation rate. The first step to try to understand the increasing trend of melt rate for increasing background rotation was to include the TC dynamics in the WC parameterization. To do so, instead of using the free stream velocity U, the area average velocity over the base of the cylindrical obstacle of the analytical steady solutions of the TC problem of section 2.2, $\overline{U}$, is used to calculate the parameterized SMR shown with the red line. Going from right to left, namely going towards higher f, there is a small peak in the melt rate, due to the relative increase in velocity on one of the side of the obstacle (see figure 3), but then, as the TC grows bigger, the average velocity at the base of the obstacle decreases, determining a relatively fast decrease in the melt rate, as well. The problem of such approach is that it neglects the well-known fact that the parameterization underestimates the melting as the velocity vanishes. To avoid that, the value of the threshold velocity U_{thr} determined above is replaced in the analytical solution pointwise wherever the velocity magnitude drops below the value U_{thr} itself and then the area average of this effective field is found, U^*. The effect of such correction on the SMR is shown by the blue line, together with the uncertainty associated to the U_{thr} itself. It still underestimates the experimental data, but the increasing trend as α decreses is captured. It is important to underline that this last threshold correction is done only in terms of the melt rate and there is no claim on the description of the effective velocity field due to the meltwater pool that accumulates at the base of the obstacle.

Figures 9 and 10 show the data points of the series of experiments with $U = 2$ cm s^{-1} and $U = 6$ cm s^{-1}, respectively, together with the same curves introduced in figure 8. While for $U = 2$ cm s^{-1}, the velocity is always below threshold and thus there is not a strong dependence on the rotation rate neither in the experimental data points nor in the corrected velocity U^* parameterization, which agree quite well, for $U = 6$ cm s^{-1} the trend in the data points as a function of α is stronger and the U^* parameterized curve is further below the data with respect to the case with $U = 4$ cm s^{-1}.

This is an indication that some other mechanism is happening at the base of the ice block and it is still not described in the parameterization. A possible explanation for that comes by looking a figure 11, which shows two pictures of the bottom of the ice blocks after two different experiments with the same $U = 4$ cm s^{-1}, but different background rotation: the left panel shows the ice block after an experiment with low f and the right panel with high f. One has to imagine that the flow was coming from the top of the picture, with the velocity radially increasing in the tank from right to left. Even if no quantitative measurements were done, this picture clearly shows that with the same relative speed U, the melting at the base of the ice block was higher for the experiment with high f with respect to the one with low f. In particular, the melting was enhanced on the outer edge of the block, because of the relative increase in velocity on one side of the cylinder at low α, as shown in figure 3. This physically explains in general the trend of increasing melt rate as the background rotation increases for the various U. But by taking a closer look to the pictures, one might notice that in the case of high background rotation rate, the melting

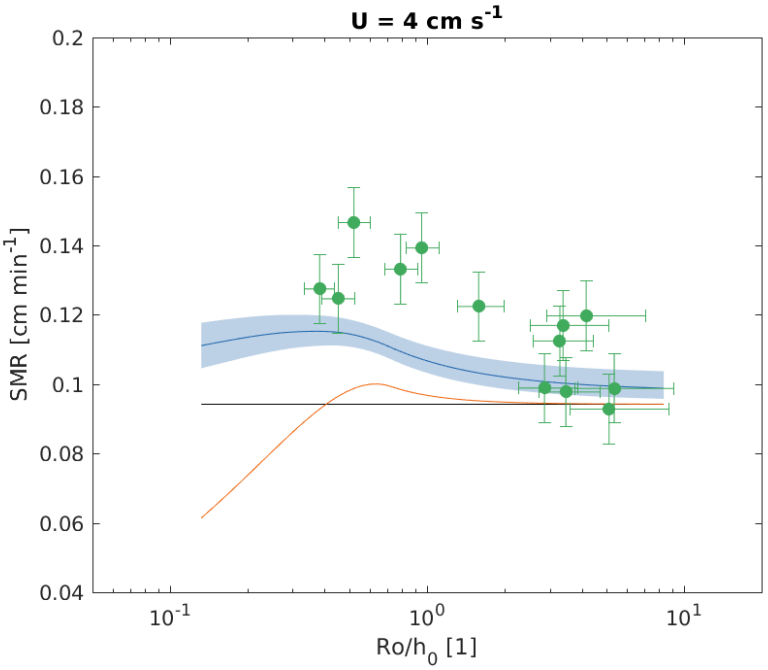

Figure 8: SMR as a function of α for $U = 4$ cm s^{-1}. The black constant line is the WC parameterization; the red line includes the TC dynamics using the parameterization the area average velocity magnitude of the analytical solution of the TC problem, $\overline{U}$; and the blue line includes both the TC dynamics and the threshold behavior observed in figure 7 applied pointwise before taking the velocity area average to find the corrected velocity U^*. See the text for further details.

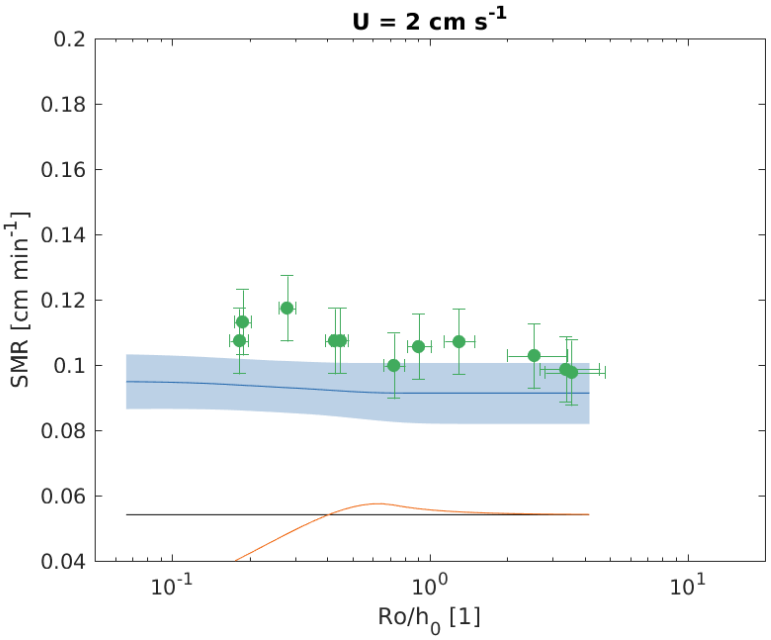

Figure 9: As in figure 8 but for $U = 2$ cm s^{-1}.

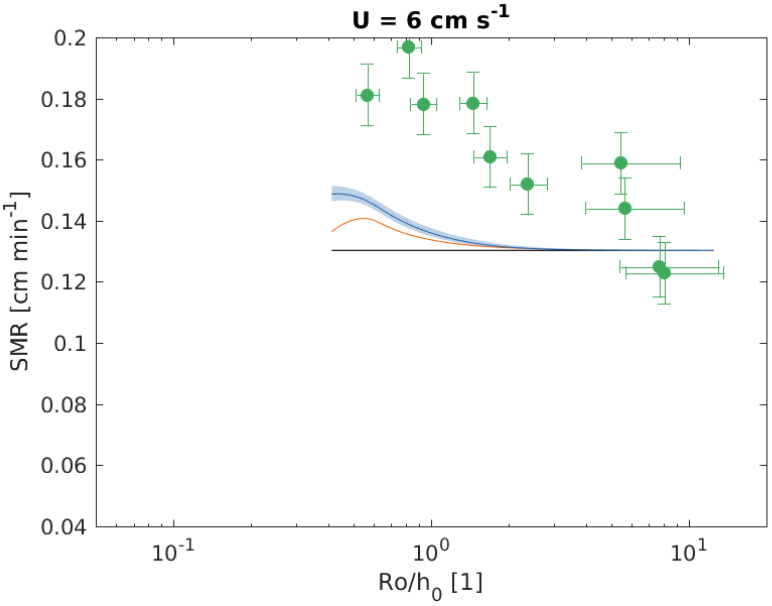

Figure 10: As in figure 8 but for $U = 6$ cm s^{-1}.

Figure 11: Two pictures of the bottom of the ice blocks after two experiments with the same free stream velocity $U = 4$ cm s^{-1}. In the left panel the rotation rate was lower than the one in the right panel and, in particular, a partial TC was observed in the experiment of the right picture, which was not the case in the experiment of the left one. Wider and deeper elongated melted stripes are visible in the right panel, due to the increased velocity at the base of the ice block determined by the TC dynamics.

happens along some elongated stripes, which are more numerous, deeper and wider than in the case of low background rotation. This suggests that some form of instability growth linked to this little channel might explain the extra melting that the parameterization is not able to explain.

Finally, figure 12 is the same as figure 6 but with the corrected velocity U^*, which takes into account both the TC dynamics and the threshold behavior observed in figure 7, instead of the free stream one, U. The data points have different shape to distinguish their free stream velocity and one can see that, although the agreement is still not very good, especially for the very low α high free stream velocity U data, the WC parameterization calculated with the corrected velocity U^* captures the increased melting at high rotation rate and the threshold behavior better than the same parameterization with the free stream velocity U.

5 Conclusions

Through laboratory experiments in a rotating tank with cylindrical ice blocks mimicking Antarctica tabular icebergs, the effects of background rotation on iceberg melting were investigated. Preliminary results show that at high rotation rate, the base of the ice block melts at a higher rate because of an increased average basal velocity below the block itself. This results from the enhanced relative vorticity below the block following the squeezing of the fluid column in the rotating system. In particular, at low background rotation, the fluid flow is almost unaffected. When increasing the rotation, i.e. lowering α, the ratio of the Rossby number and the non-dimensional height of the obstacle, the TC starts forming on one side of the obstacle and partially covers its base. In this condition, where the TC

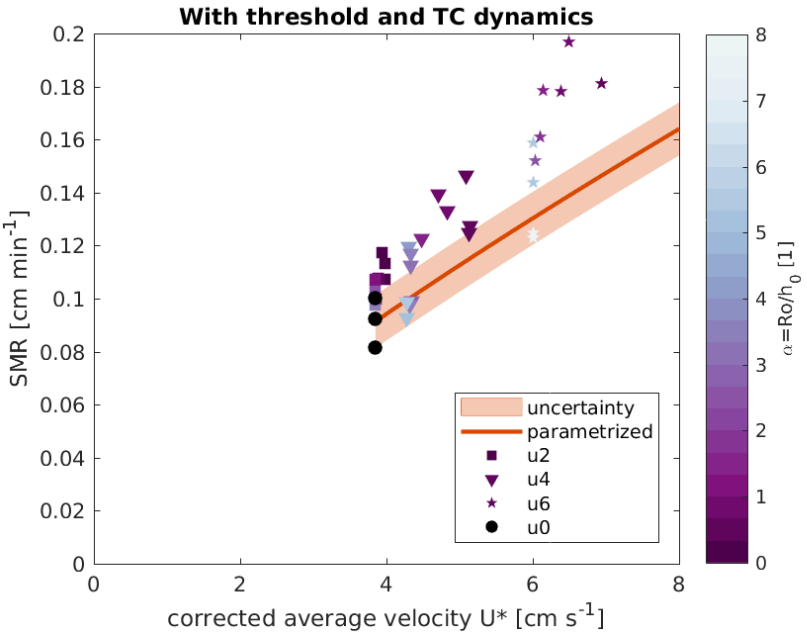

Figure 12: Similarly to figure 6, the SMR is shown as a typical velocity, which here is the corrected velocity U^* which takes into account both the TC dynamics and the threshold behavior observed above, instead of the free stream velocity U, as was in figure 6.

is not present, the flow velocity is larger than the far-field value, which is thought to be responsible for the observed higher melting. At even higher background rotation, i.e. lower α, the TC extends its area until it covers the entire ice block base. It is expected, then, that the melt rate is no longer dependent on the rotation rate, because the TC dynamics do not modify the flow structure anymore.

The WC parameterization [21] is then applied to describe the trend of the SMR as a function of the free stream velocity U. It is observed that for low relative velocity, below a certain threshold U_{thr}, the basal melt is not controlled by the forced convection due to U, but it is probably controlled by a form of upside-down gravity current formed by the buoyant meltwater pool that shields the ice block from the external fluid flow. More work is needed to better understand what is happening in this region, both in a non-rotating environment and in a rotating one. Two corrections have been done to the WC parameterization to include the TC dynamics and the observed change in regime at low relative free stream velocity. Given the analytical steady solution for the velocity magnitude below a cylindrical obstacle in a rotating frame of reference $u_{TC}(x, y)$ [12, 13], wherever its value falls below the threshold velocity U_{thr}, it is replaced by U_{thr} itself. Then, the area average of this corrected velocity field over the base of the obstacle U^* is used as effective velocity in the WC parameterization, resulting in a better agreement between data and theory.

However, some aspects of the dynamics that are thought to be important are yet to be included in the description of the process. Among the others, there are: the effects of the meltwater on the TC dynamics through changes in the stratification, which are known to introduce a dependence of the velocity on the height [11]; the curvature of

the streamlines due to the geometrical shape of the tank; the time transient features of the flow response and the turbulence added in the flow by the finiteness of the cylindrical obstacle. The possibility of an unstable growth of the melted channels at the base of the block (see figure 11) might partially explain the higher melting measured in the laboratory with respect to the parameterization, as well.

Despite a few issues that still need to be considered, the present work shows that the back-ground rotation can increase the basal melting of the large tabular icebergs due to modifi-cations of the flow typical of a rotating system and that for low relative velocity the basal melt is not controlled by the free-stream velocity.

Acknowledgments

Thanks Craig, Claudia, Bruce for the good work done together. I really learnt a lot and had a good time in the lab. Thanks Kate for the very good idea. I found it fascinating from the very beginning. Thanks Anders for the extremely precious help in building the apparatus and the ice block molds. Thanks to the lab crew, Madi, Eric, Thomasina and Earle. Thanks to the Barn crew, Robert, Federico, Guillaume and all the visitors. Thanks Margaret for the eclipse sun glasses. Thanks to the special environment of the school and to all the people that made it possible. And thanks Claudia for the suggestion of applying to the program and the continuous support.

References

[1] G. R. Bigg, *Icebergs: Their science and links to global change*, Cambridge University Press, 2015.

[2] G. R. Bigg, M. R. Wadley, D. P. Stevens, and J. A. Johnson, *Modelling dynamics and thermodynamics of icebergs*, Cold Reg. Sci. Technol., 26 (1997), pp. 113–135.

[3] G. R. Bigg and D. J. Wilton, *Iceberg risk in the Titanic year of 1912: Was it exceptional?*, Weather, 69 (2014), pp. 100–104.

[4] L. P. A. Duprat, G. R. Bigg, and D. J. Wilton, *Enhanced Southern Ocean marine productivity due to fertilization by giant icebergs*, Nat. Geosci., 9 (2016), pp. 219–221.

[5] E. R. G. Eckert and R. M. Drake, *Heat and mass transfer*, McGraw-Hill Book Co., 1959.

[6] A. FitzMaurice, C. Cenedese, and F. Straneo, *Nonlinear response of iceberg side melting to ocean currents*, Geophys. Res. Lett., 44 (2017).

[7] A. FitzMaurice, F. Straneo, C. Cenedese, and M. Andres, *Effect of a sheared flow on iceberg motion and melting*, Geophys. Res. Lett., 43 (2016), pp. 12520–12527.

[8] H. P. Greenspan and L. N. Howard, *On a time-dependent motion of a rotating fluid*, J. Fluid Mech., 17 (1963), pp. 385–404.

[9] J. J. Helly, R. S. Kaufmann, G. R. Stephenson, and M. Vernet, *Cooling, dilution and mixing of ocean water by free-drifting icebergs in the Weddell Sea*, Deep-Sea Res. II, 58 (2011), pp. 1346–1363.

[10] D. M. Holland and A. Jenkins, *Modeling thermodynamic ice-ocean interactions at the base of an ice shelf*, J. Phys. Oceanogr., 29 (1999), pp. 1787–1800.

[11] H. E. Huppert, *Some remarks on the initiation of inertial Taylor columns*, J. Fluid Mech., 67 (1975), pp. 397–412.

[12] A. P. Ingersoll, *Inertial Taylor columns and Jupiter's Great Red Spot*, J. Atmos. Sci., 26 (1969), pp. 744–752.

[13] E. R. Johnson, *Taylor columns in horizontally sheared flow*, Geophys. Astrophys. Fluid Dynamics, 24 (1983), pp. 143–164.

[14] T. Rackow, C. Wesche, R. Timmermann, H. H. Hellmer, S. Juricke, and T. Jung, *A simulation of small to giant Antarctic iceberg evolution: Differential impact on climatology estimates*, J. Geophys. Res. Oceans, 122 (2017), pp. 3170–3190.

[15] S. B. Savage, *Aspects of iceberg deterioration and drift*, in LNP 582: Geomorphological fluid mechanics, N. J. Balmforth and A. Provenzale, eds., Springer-Verlag Berlin Heidelberg, 2001, pp. 279–318.

[16] K. L. Smith, B. H. Robison, J. J. Helly, R. S. Kaufmann, H. A. Ruhl, T. J. Shaw, B. S. Twining, and M. Vernet, *Free-drifting icebergs: Hot spots of chemical and biological erichment in the Weddell Sea*, Science, 317 (2007), pp. 478–482.

[17] G. R. Stephenson, J. Sprintall, S. T. Gille, M. Vernet, J. J. Helly, and R. S. Kaufmann, *Subsurface melting of a free-floating Antarctic iceberg*, Deep-Sea Res. II, 58 (2015), pp. 1336–1345.

[18] A. A. Stern, A. Adcroft, and O. Sergienko, *The effects of Antarctic iceberg calving-size distribution in a global climate model*, J. Geophys. Res. Oceans, 121 (2016), pp. 5773–5788.

[19] G. I. Taylor, *Experiments on the motion of solid bodies in rotating fluids*, Proc. Royal Soc. A, 104 (1923), pp. 213–220.

[20] R. Timmermann, Q. Wang, and H. H. Hellmer, *Ice shelf basal melting in a global finite-element sea ice-ice shelf-ocean model*, Ann. Glaciol., 53 (2012), pp. 303–314.

[21] W. F. Weeks and W. J. Campbell, *Icebergs as a fresh-water source: an appraisal*, J. Glaciol., 12 (1973), pp. 207–233.